

Possible charge instabilities in two-dimensional doped Mott insulators

Matías Bejas*, Andrés Greco[†], and Hiroyuki Yamase[‡]

**The Abdus Salam International Centre for Theoretical Physics,
Strada Costiera 11, 34151 Trieste, Italy*

*†Facultad de Ciencias Exactas, Ingeniería y Agrimensura
and Instituto de Física Rosario (UNR-CONICET),
Av. Pellegrini 250, 2000 Rosario, Argentina*

‡National Institute for Materials Science, Tsukuba 305-0047, Japan

‡Max-Planck-Institute for Solid State Research, D-70569 Stuttgart, Germany

(Dated: July 16, 2012)

Abstract

Motivated by the growing evidence of the importance of charge fluctuations in the pseudogap phase in high-temperature cuprate superconductors, we apply a large- N expansion formulated in a path integral representation of the two-dimensional t - J model on a square lattice. We study all possible charge instabilities of the paramagnetic state in leading order of the $1/N$ expansion. While the d -wave charge density wave (flux phase) becomes the leading instability for various choices of model parameters, we find that a d -wave Pomeranchuk (electronic nematic phase) instability occurs as a next leading one. In particular, the nematic state has a strong tendency to become inhomogeneous. In the presence of a large second nearest-neighbor hopping integral, the flux phase is suppressed and the electronic nematic instability becomes leading in a high doping region. Besides these two major instabilities, bond-order phases occur as weaker instabilities close to half-filling. Phase separation is also detected in a finite temperature region near half-filling.

PACS numbers: 71.10.Hf, 74.72.Gh, 74.72.Kf

I. INTRODUCTION

The pseudogap (PG) phase in cuprate superconductors provides one of the most active subjects on high- T_c superconductivity. The PG phase is characterized by highly anomalous properties^{1,2} which are rather universal for all cuprate superconductors. One of the puzzling observations comes from angle-resolved photoemission spectroscopy (ARPES) measurements,³ which revealed arc-shaped disconnected Fermi surfaces,⁴ called Fermi arcs, instead of a large Fermi surface. In underdoped cuprates the PG opens below a temperature T^* , which is far above the superconducting transition temperature T_{sc} . Furthermore, in contrast to the behavior of T_{sc} , T^* increases with decreasing doping in the underdoped region. The PG is very anisotropic along the Fermi surface. It has a maximal gap in the $(0,0)$ - $(0,\pi)$ direction (antinodal direction) and vanishes upon approaching the Brillouin zone diagonal (nodal direction), similar to the d -wave superconducting gap.

In spite of the consensus on the existence of the PG, its origin and nature remain elusive. There are two major scenarios. One is that the PG originates from preformed pairs above T_{sc} .^{5,6} The other is that the PG is distinct from the superconducting gap and associated with a certain order which competes with superconductivity, but both coexist at low temperature, leading to “two gaps” in the electronic spectrum.⁷⁻⁹ Several phenomenological models which are in favor of the two-gap scenario were already studied in various contexts, but invoking different orders, such as d -wave charge density wave (d CDW),¹⁰ d -wave Fermi surface deformations,¹¹ charge density wave¹²⁻¹⁵ including stripes,^{16,17} phase separation (PS),^{12,13,18} and others such as resonating-valence-bond-type charge order¹⁹ and loop-current order.²⁰

The d CDW is a flux phase, where orbital currents flow around each plaquette in a staggered pattern. The electronic spectrum in the flux phase has a gap with d -wave symmetry, the same as the superconducting gap symmetry. The flux phase was obtained in the large- N approach to the t - J model in various formalisms²¹⁻²⁵ and the presence of flux correlations was confirmed by the exact diagonalization.²⁶ On the other hand, in the Hubbard model, the dynamical cluster approximation failed to detect static long-range order of the d CDW²⁷ whereas the variational cluster approximation showed that the d CDW is a metastable solution.²⁸ Fluctuations associated with the d CDW can provide a route to address the PG. A perturbative analysis of the electron self-energy due to d CDW fluctuations catches many important features observed by ARPES, not only a PG and its associated

Fermi arcs^{29,30} but also a semiquantitative aspect of renormalization of the electron band dispersion in the PG phase.³¹

The d -wave Fermi surface deformations are driven by a d -wave Pomeranchuk³² instability (d PI), leading to an electronic nematic state.³³ In this state, an orientational symmetry of the systems is broken without breaking however translational invariance. The d PI was found in the slave-boson mean-field,³⁴ exact diagonalization,³⁵ and variational Monte Carlo³⁶ studies in the t - J model, and also in the Hubbard model.^{37–39} The d PI itself does not become the leading instability in most of theoretical studies. However, it was pointed out that the models retain appreciable correlations of the d PI,^{34,40} which then may lead to a giant response to a small xy anisotropy. Such a giant response was actually observed in the PG region in $\text{YBa}_2\text{Cu}_3\text{O}_y$, which has a small anisotropy originating from the orthorhombic crystal structure, by neutron scattering^{41,42} and transport measurements.⁴³ Theoretical studies for the former^{11,44} and the latter⁴⁵ confirmed that idea.

Charge-stripe order is extensively discussed for cuprates.^{16,17} Since the charge-stripe order breaks both orientational and translational symmetry of the system, the stripe phase is also called an electronic smectic phase³³ and has lower symmetry than the nematic phase. The experimental observation of charge order in La-based cuprates⁴⁶ provides grounds to consider the stripe order. A charge-stripe solution was indeed obtained in the density matrix renormalization group (DMRG) study^{47,48} in the t - J model. However in the presence of the second nearest-neighbor hopping integral the charge-stripe order turned out to be unstable in the t - J model.^{49,50}

PS is also another possible instability in the t - J model.^{51,52} It is however still highly debated whether the model indeed shows the instability toward PS^{53,54} or not^{47,48,55–59} in a parameter region realistic to cuprates. Although PS is in general suppressed by long-range Coulomb forces, strong charge fluctuations in the proximity to PS can be important and responsible for anomalous properties in the PG phase and superconductivity.¹⁸ In fact, the proximity to PS plays an important role to generate a singular interaction between electrons at zero momentum transfer as shown in the infinite- U Hubbard Holstein model.^{12,13} When long-range Coulomb interactions are added, the singularity shifts to a finite momentum transfer, leading to an incommensurate charge density wave similar to stripes.^{12,13}

Theoretically it is believed that the two-dimensional (2D) t - J and Hubbard models contain the main ingredients for describing cuprates,⁶⁰ i.e., antiferromagnetism at zero doping,

a metallic state at finite doping, and a strong tendency to d -wave superconductivity. Given that various charge instabilities are invoked to address the PG, and also other anomalous properties in cuprates, it is interesting to study what kind of charge instabilities are favored in the 2D t - J model by treating all possibilities on equal footing in a controllable scheme.

In this paper, we analyze the 2D t - J model in terms of Hubbard operators by including the nearest-neighbor Coulomb interaction V to avoid a subtle feature of PS; our main results are not affected by the presence of V . We apply a large- N expansion formulated in a path integral representation.^{25,61,62} In this approach the two spin components are extended to N and an expansion in powers of the small parameter $1/N$ is performed, providing a controllable scheme without a perturbative expansion in any model parameter. In addition, different kind of instabilities can be studied on equal footing, allowing us to perform a stability analysis on all possible charge instabilities already at leading order. We find that the t - J model shows tendencies to the flux and electronic nematic state in a wide doping region. In particular, the nematic state has a strong tendency to become inhomogeneous. Close to half-filling, bond-order phase (BOP) and PS are also obtained.

In the next section, we first provide a brief summary of our theoretical scheme and then explain the most important charge instabilities, d CDW, d PI, BOP, and PS. Our results are presented in Sec. III and are discussed by comparing with literature in Sec. IV. Implications for cuprates are also discussed in the same section.

II. THEORETICAL FRAMEWORK

A. Large- N approach to the t - J - V model

In a previous paper,²⁵ a large- N expansion for the t - J - V model was formulated in terms of a path integral representation for the Hubbard X -operators. For the sake of a self-contained presentation, we first summarize the formalism.

The t - J - V model is described by the following Hamiltonian,

$$H = - \sum_{i,j,\sigma} t_{ij} \tilde{c}_{i\sigma}^\dagger \tilde{c}_{j\sigma} + J \sum_{\langle i,j \rangle} (\vec{S}_i \cdot \vec{S}_j - \frac{1}{4} n_i n_j) + V \sum_{\langle i,j \rangle} n_i n_j, \quad (1)$$

where $t_{ij} = t$ (t') is the hopping integral between the first (second) nearest-neighbor sites on a square lattice; J and V are the exchange interaction and the Coulomb repulsion,

respectively, between the nearest-neighbor sites. The main role of the V -term in the present study is to suppress the tendency toward PS while, in other works,^{63,64} the V -term was included to investigate its effect on superconductivity. $\tilde{c}_{i\sigma}^\dagger$ and $\tilde{c}_{i\sigma}$ are the creation and annihilation operators of electrons with spin σ ($\sigma = \downarrow, \uparrow$), respectively, under the constraint that the double occupancy of electrons is excluded at any site i . n_i is the electron density operator.

The electron and spin operators are connected to Hubbard operators⁶⁵ via $\tilde{c}_{i\sigma}^\dagger = X_i^{\sigma 0}$, $\tilde{c}_{i\sigma} = X_i^{0\sigma}$, $S_i^+ = X_i^{\uparrow\downarrow}$, $S_i^- = X_i^{\downarrow\uparrow}$, and $n_i = X_i^{\uparrow\uparrow} + X_i^{\downarrow\downarrow}$. The operators $X_i^{\sigma 0}$ and $X_i^{0\sigma}$ are called fermionlike, whereas the operators $X_i^{\sigma\sigma'}$ and X_i^{00} are called bosonlike; X_i^{00} will be introduced later [Eq. (4)]. After writing Hamiltonian (1) in terms of the Hubbard operators, we extend the spin degree of freedom to N channels and obtain the Hamiltonian in the large- N formalism,

$$H = -\frac{1}{N} \sum_{i,j,p} t_{ij} X_i^{p0} X_j^{0p} + \frac{J}{2N} \sum_{\langle i,j \rangle, pp'} (X_i^{pp'} X_j^{p'p} - X_i^{pp} X_j^{p'p'}) + \frac{V}{N} \sum_{\langle i,j \rangle, pp'} X_i^{pp} X_j^{p'p'} - \mu \sum_{i,p} X_i^{pp}. \quad (2)$$

The spin index σ is extended to a new index p , which runs from 1 to N . In order to obtain a finite theory in the N -infinite limit, t , t' , J and V are rescaled as t/N , t'/N , J/N and V/N , respectively. The chemical potential μ is introduced in Eq. (2).

In the path integral formulation our Euclidean Lagrangian reads

$$L_E = \frac{1}{2} \sum_{i,p} \frac{(\dot{X}_i^{0p} X_i^{p0} + \dot{X}_i^{p0} X_i^{0p})}{X_i^{00}} + H \quad (3)$$

with the following two additional constraints,

$$X_i^{00} + \sum_p X_i^{pp} - \frac{N}{2} = 0, \quad (4)$$

and

$$X_i^{pp'} - \frac{X_i^{p0} X_i^{0p'}}{X_i^{00}} = 0, \quad (5)$$

which are imposed on the path integral via two δ -functions. In Eq. (3), $\dot{X}_i^{p0} = \partial_\tau X_i^{p0}$ and τ is the euclidean time, namely $\tau = it$. Equation (4) is the N -extended completeness condition. The form of the kinetic term in the Lagrangian L_E , as well as the constraint Eq. (5), comes from the requirement that the X -operators should fulfill their commutation

rules. For details we refer to Ref. 61. In the path integral approach we associate Grassmann and usual bosonic variables with fermionlike and bosonlike X -operators, respectively.

We now discuss the main steps needed to introduce a large- N expansion.^{25,62} First the V -term in the Hamiltonian is written in terms of X_i^{00} by using Eq. (4). We then eliminate the bosonic variables $X^{pp'}$ by implementing the δ -function associated with Eq. (5). The completeness condition [Eq. (4)] is imposed by introducing Lagrange multipliers λ_i . We write X_i^{00} and λ_i in terms of static mean-field values, r_0 and λ_0 , and fluctuation fields, δR_i and $\delta \lambda_i$,

$$\begin{aligned} X_i^{00} &= N r_0 (1 + \delta R_i) \\ \lambda_i &= \lambda_0 + \delta \lambda_i. \end{aligned} \quad (6)$$

In addition, we introduce the following fermion fields⁶⁶ defined by

$$\begin{aligned} f_{ip}^\dagger &= \frac{1}{\sqrt{N r_0}} X_i^{p0}, \\ f_{ip} &= \frac{1}{\sqrt{N r_0}} X_i^{0p}. \end{aligned} \quad (7)$$

The exchange interaction is then described by four fermion fields, which are decoupled through a Hubbard-Stratonovich transformation by introducing a field associated with a bond variable,

$$\Delta_{ij} = J \sum_p \frac{f_{jp}^\dagger f_{ip}}{\sqrt{(1 + \delta R_i)(1 + \delta R_j)}}. \quad (8)$$

The field Δ_{ij} is parameterized by

$$\Delta_i^\eta = \Delta (1 + r_i^\eta + i A_i^\eta), \quad (9)$$

where r_i^η and A_i^η correspond to the real and imaginary parts of the fluctuations of the bond variable, respectively, and Δ is a static mean-field value. The index η takes two values associated with the bond directions $\eta_1 = (1, 0)$ and $\eta_2 = (0, 1)$ on a square lattice. After expanding $1/(1 + \delta R)$ in powers of δR , we obtain an effective Lagrangian, which can be written in terms of a six-component boson field

$$\delta X^a = (\delta R, \delta \lambda, r^{\eta_1}, r^{\eta_2}, A^{\eta_1}, A^{\eta_2}), \quad (10)$$

the fermions f_p , and their interactions.

From the quadratic part for fermions we obtain an electronic propagator in the paramagnetic phase,

$$G(\mathbf{k}, i\nu_n) = \frac{1}{i\nu_n - \varepsilon_{\mathbf{k}}} . \quad (11)$$

Here \mathbf{k} and $i\nu_n$ are the momentum and fermionic Matsubara frequency, respectively, and the electronic dispersion $\varepsilon_{\mathbf{k}}$ is

$$\varepsilon_{\mathbf{k}} = -2(tr_0 + \Delta)(\cos k_x + \cos k_y) - 4t'r_0 \cos k_x \cos k_y - \mu . \quad (12)$$

Here λ_0 in Eq. (6) was absorbed in the chemical potential μ .

From the completeness condition [Eq. (4)] r_0 is equal to $\delta/2$, where δ is the hole doping rate away from half-filling. The field Δ is given by the expression

$$\Delta = \frac{J}{4N_s} \sum_{\mathbf{k}, \eta} \cos(k_\eta) n_F(\varepsilon_{\mathbf{k}}) , \quad (13)$$

where n_F is the Fermi function and N_s is the total number of lattice sites. For a given doping, μ and Δ are determined self-consistently by solving Eq. (13) and

$$(1 - \delta) = \frac{2}{N_s} \sum_{\mathbf{k}} n_F(\varepsilon_{\mathbf{k}}) . \quad (14)$$

The quadratic part for δX^a defines a 6×6 bare bosonic propagator $D_{ab}^{(0)}(\mathbf{q}, i\omega_n)$, which after Fourier transformation reads,

$$[D_{ab}^{(0)}(\mathbf{q}, i\omega_n)]^{-1} = N \begin{pmatrix} \frac{\delta^2}{2} (V - \frac{J}{2}) [\cos(q_x) + \cos(q_y)] & \frac{\delta}{2} & 0 & 0 & 0 & 0 \\ \frac{\delta}{2} & 0 & 0 & 0 & 0 & 0 \\ 0 & 0 & \frac{4\Delta^2}{J} & 0 & 0 & 0 \\ 0 & 0 & 0 & \frac{4\Delta^2}{J} & 0 & 0 \\ 0 & 0 & 0 & 0 & \frac{4\Delta^2}{J} & 0 \\ 0 & 0 & 0 & 0 & 0 & \frac{4\Delta^2}{J} \end{pmatrix} , \quad (15)$$

where \mathbf{q} and $i\omega_n$ are the momentum and bosonic Matsubara frequency, respectively. The quantity $D_{ab}^{(0)}(\mathbf{q}, i\omega_n)$ describes all possible types of bare charge susceptibilities. The bare susceptibilities are renormalized already at leading order to become dressed ones, which are given by the Dyson equation

$$D_{ab}^{-1}(\mathbf{q}, i\omega_n) = [D_{ab}^{(0)}(\mathbf{q}, i\omega_n)]^{-1} - \Pi_{ab}(\mathbf{q}, i\omega_n) . \quad (16)$$

Following the diagrammatic rules in Ref. 25, the 6×6 boson self-energies Π_{ab} are computed as

$$\begin{aligned} \Pi_{ab}(\mathbf{q}, i\omega_n) = & -\frac{N}{N_s} \sum_{\mathbf{k}} h_a(\mathbf{k}, \mathbf{q}, \varepsilon_{\mathbf{k}} - \varepsilon_{\mathbf{k}-\mathbf{q}}) \frac{n_F(\varepsilon_{\mathbf{k}-\mathbf{q}}) - n_F(\varepsilon_{\mathbf{k}})}{i\omega_n - \varepsilon_{\mathbf{k}} + \varepsilon_{\mathbf{k}-\mathbf{q}}} h_b(\mathbf{k}, \mathbf{q}, \varepsilon_{\mathbf{k}} - \varepsilon_{\mathbf{k}-\mathbf{q}}) \\ & - \delta_{a1} \delta_{b1} \frac{N}{N_s} \sum_{\mathbf{k}} \frac{\varepsilon_{\mathbf{k}} - \varepsilon_{\mathbf{k}-\mathbf{q}}}{2} n_F(\varepsilon_{\mathbf{k}}) . \end{aligned} \quad (17)$$

The prefactor N in front of the right hand side of Eq. (17) comes from the sum over the N channels of p . Thus, the 6×6 boson self-energies Π_{ab} are of the same order as $[D_{ab}^{(0)}]^{-1}$ [see Eq. (15)]. In Eq. (17) h_a is an effective six-component interaction vertex which comes from the interaction terms between bosonic and fermionic fields derived from the effective Lagrangian. The explicit expression for h_a is given by

$$\begin{aligned} h_a(\mathbf{k}, \mathbf{q}, \nu) = & \left\{ \frac{2\varepsilon_{\mathbf{k}-\mathbf{q}} + \nu + 2\mu}{2} + 2\Delta \left[\cos\left(k_x - \frac{q_x}{2}\right) \cos\left(\frac{q_x}{2}\right) + \cos\left(k_y - \frac{q_y}{2}\right) \cos\left(\frac{q_y}{2}\right) \right] ; 1 ; \right. \\ & \left. -2\Delta \cos\left(k_x - \frac{q_x}{2}\right) ; -2\Delta \cos\left(k_y - \frac{q_y}{2}\right) ; 2\Delta \sin\left(k_x - \frac{q_x}{2}\right) ; 2\Delta \sin\left(k_y - \frac{q_y}{2}\right) \right\} . \end{aligned} \quad (18)$$

From the N -extended completeness condition [Eq. (4)] we see that the charge operator X^{00} is $O(N)$, while the operators X^{pp} are $O(1)$. Consequently, the $1/N$ approach emphasizes the effective charge interactions. In fact, while in leading order charge susceptibilities contain collective effects, they enter the spin susceptibilities in the next-to-leading order. Similarly, superconductivity appears in the next-to-leading order.^{24,63} Therefore, instabilities of the paramagnetic phase are expected only, in leading order, in the charge sector.

In leading order, our formalism agrees with the $1/N$ slave-boson formalism.²³ However, in the present approach the fermion variables f_{ip} are proportional to the X -operators [Eq. (7)] and should not be confused with the spinons in the slave-boson approach. In addition, δR [Eq. (6)] is proportional to charge fluctuations and not related to holons. Since the X -operators are treated as fundamental objects, problems associated with fluctuations of gauge fields in the slave-boson approach⁶⁷ are avoided. Our formalism was also checked to yield results consistent with the exact diagonalization^{68,69} as well as results in another formalism of the $1/N$ expansion in leading order.²⁴

B. Instabilities of the paramagnetic phase

An instability of the paramagnetic phase is signaled by the divergence of the static susceptibilities defined by $D_{ab}(\mathbf{q}, i\omega_n)$ for a continuous phase transition. Therefore we study eigenvalues and eigenvectors of the matrix $[D_{ab}(\mathbf{q}, i\omega_n)]^{-1}$ at $i\omega_n = 0$. When an eigenvalue crosses zero at a given doping rate, temperature T , and momentum \mathbf{q} , an instability occurs toward a phase characterized by the corresponding eigenvector. We have found five instabilities associated with eigenvectors V^a explained below.

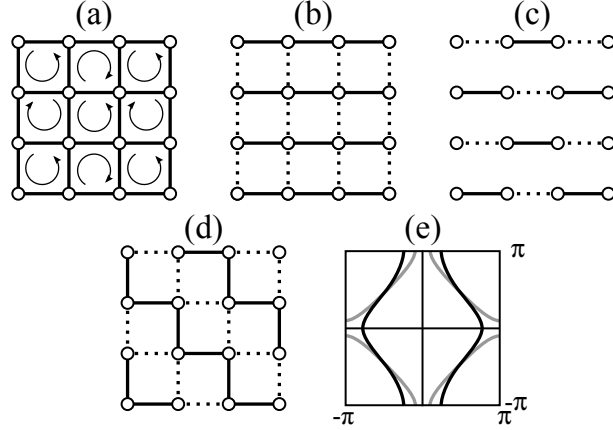


FIG. 1: Sketch of various phases appearing in our work. Commensurate orders for (a) d CDW, (b) d PI, (c) BOP_x , and (d) BOP_{xy} in real space. The commensurate d PI has a momentum $\mathbf{q} = (0, 0)$ whereas the commensurate d CDW, BOP_x , and BOP_{xy} have $\mathbf{q} = (\pi, \pi)$. Solid and dashed lines in (b)-(d) represent the strong and weak bonds, respectively. (e) Fermi surface deformations (black line) associated with the commensurate d PI; the original Fermi surface is sketched by gray lines.

a) $V^a = \frac{1}{\sqrt{2}}(0, 0, 0, 0, 1, -1)$, which corresponds to the freeze of the imaginary parts of the bond variable [Eq. (9)]. The pure imaginary contribution to the hopping term generates a net magnetic flux in each plaquette, leading to the instability toward the flux or d CDW phase as already found previously.^{21–25} The commensurate flux phase is characterized by the modulation vector $\mathbf{q} = (\pi, \pi)$ and describes staggered circulating currents as sketched in Fig. 1 (a), whereas the incommensurate phase is characterized by $\mathbf{q} \neq (\pi, \pi)$.

b) $V^a = \frac{1}{\sqrt{2}}(0, 0, 1, -1, 0, 0)$, which corresponds to the freeze of the real parts of the bond variable. This eigenvector corresponds to the commensurate [$\mathbf{q} = (0, 0)$] or incommensurate [$\mathbf{q} \neq (0, 0)$] instability toward the d PI phase. The commensurate phase is sketched in Fig. 1 (b) in real space. In momentum space it leads to Fermi surface deformations where the

Fermi surface expands along the k_y direction and shrinks along the k_x direction [Fig. 1 (e)], or vice versa if the bond along the y direction would become stronger than the x direction. While the commensurate d PI has been discussed since 2000,^{34,37} an incommensurate d PI starts to be discussed very recently.^{70–73}

c) $V^a = (0, 0, 1, 0, 0, 0)$ $((0, 0, 0, 1, 0, 0))$, which correspond to the freeze of the third (fourth) component and describe the instability toward the BOP_x (BOP_y).^{23–25} The corresponding modulation vector turns out to be $\mathbf{q} = (\pi, \pi)$ or very close to it. The commensurate BOP_x , namely with $\mathbf{q} = (\pi, \pi)$, is sketched in Fig. 1 (c) whereas the BOP_y with $\mathbf{q} = (\pi, \pi)$ is obtained by rotating Fig. 1 (c) by 90° .

d) $V^a = \frac{1}{\sqrt{2}}(0, 0, 1, 1, 0, 0)$, which corresponds to the freeze of both third and fourth components simultaneously. The modulation vector is $\mathbf{q} = (\pi, \pi)$ or very close to it, as in the case of the BOP_x and BOP_y . We refer to this instability as the BOP_{xy} . The commensurate BOP_{xy} with $\mathbf{q} = (\pi, \pi)$ is sketched in Fig. 1 (d). For simplicity, we also use the phrase BOP when we do not have to distinguish between BOP_x , BOP_y , and BOP_{xy} .

e) $V^a = (1, 0, 0, 0, 0, 0)$, which corresponds to the freeze of charge fluctuations δR and describes the instability toward PS for $\mathbf{q} = (0, 0)$ and a charge-density-wave phase, including stripes, for a finite \mathbf{q} . A finite \mathbf{q} instability, however, was not detected in the present study.

In general, eigenvectors of $[D_{ab}(\mathbf{q}, i\omega_n)]^{-1}$ can have a non-zero value in each component. However we checked that the inner product between an eigenvector of $[D_{ab}(\mathbf{q}, i\omega_n)]^{-1}$ and V^a becomes larger than 0.99 at the corresponding critical point.

C. Effective susceptibilities

While numerical results presented in this paper are computed from the full susceptibility Eq. (16), it is instructive to extract an effective susceptibility associated with each instability explained in the previous section by discarding the interactions with other modes contained in $D_{ab}(\mathbf{q}, i\omega_n)$.

The usual charge-charge correlation function is written as

$$\chi_{ij}^c(\tau) = \frac{1}{N} \sum_{p,q} \langle T_\tau X_i^{pp}(\tau) X_j^{qq}(0) \rangle. \quad (19)$$

Using the completeness condition [Eq. (4)] and the relation between X_i^{00} and δR_i [Eq. (6)],

χ_{ij}^c can be written in Fourier space,²⁵

$$\chi^c(\mathbf{q}, i\omega_n) = -N \left(\frac{\delta}{2} \right)^2 D_{11}(\mathbf{q}, i\omega_n). \quad (20)$$

Thus the charge-charge correlation function is just the component (1, 1) of the D_{ab} . Note that the factor N in front of the right hand side of Eq. (20) shows that charge fluctuations are of $O(1)$ since $D_{ab} \propto 1/N$ as seen in Eq. (15).

The susceptibility of the d CDW is obtained by focusing on the sector $a, b = 5, 6$ of the matrix D_{ab}^{-1} . We obtain

$$\chi_{d\text{CDW}}(\mathbf{q}, i\omega_n) = [(8/J)\Delta^2 - \Pi_{d\text{CDW}}(\mathbf{q}, i\omega_n)]^{-1}, \quad (21)$$

where $\Pi_{d\text{CDW}}(\mathbf{q}, i\omega_n)$ is the electronic polarizability of the d CDW and is given by

$$\Pi_{d\text{CDW}}(\mathbf{q}, i\omega_n) = -\frac{1}{N_s} \sum_{\mathbf{k}} \gamma_{d\text{CDW}}^2(\mathbf{q}, \mathbf{k}) \frac{n_F(\epsilon_{\mathbf{k}+\mathbf{q}}) - n_F(\epsilon_{\mathbf{k}})}{\epsilon_{\mathbf{k}+\mathbf{q}} - \epsilon_{\mathbf{k}} - i\omega_n}, \quad (22)$$

with a form factor $\gamma_{d\text{CDW}}(\mathbf{q}, \mathbf{k}) = 2\Delta[\sin(k_x + q_x/2) - \sin(k_y + q_y/2)]$.

Similarly, the susceptibility of the d PI is obtained from the sector $a, b = 3, 4$ of the matrix D_{ab}^{-1} :

$$\chi_{d\text{PI}}(\mathbf{q}, i\omega_n) = [(8/J)\Delta^2 - \Pi_{d\text{PI}}(\mathbf{q}, i\omega_n)]^{-1} \quad (23)$$

and the electronic polarizability of the d PI reads

$$\Pi_{d\text{PI}}(\mathbf{q}, i\omega_n) = -\frac{1}{N_s} \sum_{\mathbf{k}} \gamma_{d\text{PI}}^2(\mathbf{q}, \mathbf{k}) \frac{n_F(\epsilon_{\mathbf{k}+\mathbf{q}}) - n_F(\epsilon_{\mathbf{k}})}{\epsilon_{\mathbf{k}+\mathbf{q}} - \epsilon_{\mathbf{k}} - i\omega_n}, \quad (24)$$

with a form factor $\gamma_{d\text{PI}}(\mathbf{q}, \mathbf{k}) = 2\Delta[\cos(k_x + q_x/2) - \cos(k_y + q_y/2)]$.

For the case of the BOP_x we focus on the sector $a = b = 3$ and obtain

$$\chi_{\text{BOP}_x}(\mathbf{q}, i\omega_n) = [(4/J)\Delta^2 - \Pi_{\text{BOP}_x}(\mathbf{q}, i\omega_n)]^{-1}, \quad (25)$$

where the electronic polarizability is given by

$$\Pi_{\text{BOP}_x}(\mathbf{q}, i\omega_n) = -\frac{1}{N_s} \sum_{\mathbf{k}} 4\Delta^2 \cos^2(k_x + q_x/2) \frac{n_F(\epsilon_{\mathbf{k}+\mathbf{q}}) - n_F(\epsilon_{\mathbf{k}})}{\epsilon_{\mathbf{k}+\mathbf{q}} - \epsilon_{\mathbf{k}} - i\omega_n}. \quad (26)$$

For the case of $a = b = 4$, i.e., BOP_y , the form factor in Eq. (26) is replaced by $\cos^2(k_y + q_y/2)$. It is easily seen in Eq. (26) that the BOP_x and BOP_y instabilities occur simultaneously, but with a different modulation vector: suppose $\mathbf{q} = (q_x, q_y)$ for the BOP_x , then $\mathbf{q} = (q_y, q_x)$ for

the BOP_y. While we will not present results for the BOP_y, it should be understood that the instability of the BOP_y also exists.

The susceptibility associated with BOP_{xy} is given by the same equation as Eq. (23), except that the form factor γ_{dPI} in Eq. (24) is replaced by $\gamma_{BOP_{xy}}(\mathbf{q}, \mathbf{k}) = 2\Delta[\cos(k_x + q_x/2) + \cos(k_y + q_y/2)]$.

The form factor $\gamma_{dCDW}(\mathbf{q}, \mathbf{k}) [\gamma_{dPI}(\mathbf{q}, \mathbf{k})]$ has a \mathbf{k} dependence of $\cos k_x - \cos k_y$ at $\mathbf{q} = (\pi, \pi)$ [$\mathbf{q} = (0, 0)$], which indicates the *d*-wave character of the instability. Note that the *d*PI and *d*CDW belong to different eigenspace and are not connected with each other by changing the momentum \mathbf{q} .

While the terminology of the *d*PI itself makes sense when a modulation vector is close to $\mathbf{q} = (0, 0)$, we may consider formally a large \mathbf{q} in Eqs. (23) and (24). The *d*PI is then connected with the BOP_x and BOP_y when \mathbf{q} is located along the direction of $(\pi, 0)$ - (π, π) or $(0, \pi)$ - (π, π) . Suppose $\mathbf{q}' = (\pi, q_y)$, we can easily find

$$\Pi_{dPI}(\mathbf{q}', i\omega_n) = \Pi_{BOP_x}(\mathbf{q}', i\omega_n) + \Pi_{BOP_y}(\mathbf{q}', i\omega_n), \quad (27)$$

by noting that

$$\frac{1}{N_s} \sum_{\mathbf{k}} \sin k_x \cos(k_y + q_y/2) \frac{n_F(\epsilon_{\mathbf{k}+\mathbf{q}'} - \epsilon_{\mathbf{k}}) - n_F(\epsilon_{\mathbf{k}})}{\epsilon_{\mathbf{k}+\mathbf{q}'} - \epsilon_{\mathbf{k}} - i\omega_n} = 0. \quad (28)$$

We thus obtain

$$\chi_{dPI}^{-1}(\mathbf{q}', i\omega_n) = \chi_{BOP_x}^{-1}(\mathbf{q}', i\omega_n) + \chi_{BOP_y}^{-1}(\mathbf{q}', i\omega_n). \quad (29)$$

In particular, when \mathbf{q}' is equal to $\mathbf{Q} \equiv (\pi, \pi)$, Eq. (29) is reduced to

$$\chi_{dPI}(\mathbf{Q}, i\omega_n) = \frac{1}{2} \chi_{BOP_x}(\mathbf{Q}, i\omega_n), \quad (30)$$

because $\chi_{BOP_x}(\mathbf{Q}, i\omega_n) = \chi_{BOP_y}(\mathbf{Q}, i\omega_n)$. Similarly, we can also obtain

$$\chi_{dPI}(\mathbf{Q}, i\omega_n) = \chi_{BOP_{xy}}(\mathbf{Q}, i\omega_n). \quad (31)$$

Hence when the static BOP susceptibility diverges at $\mathbf{q} = (\pi, \pi)$, the *d*PI susceptibility also diverges simultaneously at the same momentum unless it already diverges at a different momentum. In fact, the *d*PI with $\mathbf{q} = (\pi, \pi)$ is equivalent to the BOP_{xy} and is interpreted as superposition of the BOP_x and BOP_y as seen in Fig. 1 (d).

III. RESULTS

We choose the parameters, $J/t = 0.3$ and $V/t = 0.5$. We set $t = 1$, and all quantities with dimension of energy are in units of t . Irrespective of the presence of the V -term, our theory catches intrinsic charge instabilities in the 2D t - J model such as d CDW, d PI, and BOP, which are driven by the J -term. We compute the full susceptibility Eq. (16) for various choices of t' by assuming the paramagnetic phase and determine possible charge instabilities in the plane of hole density δ and temperature T . At half-filling an analytical solution is obtained and the d CDW, d PI, and BOP have the same onset temperature, $T_c = J/8 = 0.0375t$, at which the static field Δ [Eq. (9)] also sets in. Away from half-filling ($\delta > 0.004$) our computation is fully numerical. Since we determine critical lines by studying the susceptibility, the transition is continuous. In other words, a possibility of a first order transition is not considered in the present analysis.

A. Results for $t' = 0$

Figure 2 shows the phase diagram for $t' = 0$. As mentioned in Sec. II.B, five different types of charge instability are found: d CDW, d PI, BOP_x , BOP_{xy} , and PS. The instability toward the commensurate d CDW, namely with $\mathbf{q} = (\pi, \pi)$, occurs in a wide doping region. The transition temperature decreases gradually with increasing hole density and exhibits reentrant behavior at low T in the region $0.12 \lesssim \delta \lesssim 0.14$. However, near $\delta \approx 0.14$ an incommensurate [$\mathbf{q} \neq (\pi, \pi)$] d CDW instability occurs below $T \approx 0.015$ and its critical doping rate is higher than that of the commensurate d CDW. Hence the resulting critical line of the d CDW follows the outer line, i.e., the thin line at low T and the thick line for high T .

For $t' = 0$ the commensurate d PI with $\mathbf{q} = (0, 0)$ has the same onset temperature as the commensurate BOP_x and BOP_{xy} , namely with $\mathbf{q} = (\pi, \pi)$; this reason will be explained in the last paragraph in the present section. The transition lines exhibit reentrant behavior at low T . However, an incommensurate d PI emerges at low T and preempts the reentrant line, extending the region of d PI. BOP_x and BOP_{xy} also exhibit an incommensurate instability at low T and preempt their commensurate instabilities. Furthermore the degeneracy between BOP_x and BOP_{xy} is lifted via an incommensurate transition. While the critical doping rate

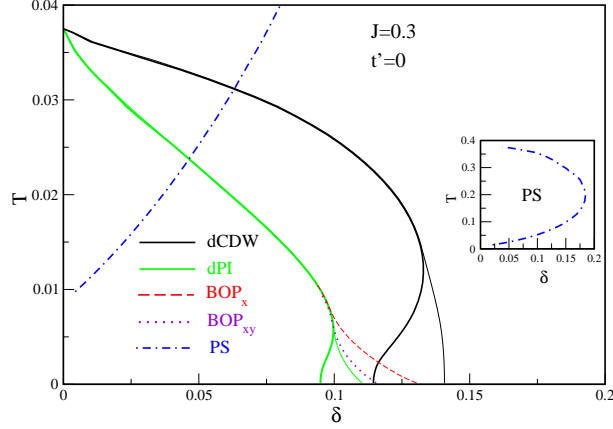


FIG. 2: (Color online) Critical temperature versus doping rate for $dCDW$, dPI , BOP_x , BOP_{xy} , and PS for $t' = 0$ and $J = 0.3$. Thick (thin) lines describe commensurate (incommensurate) transitions. The critical line for PS is shown in a larger scale of T in the inset.

for BOP becomes higher than for dPI at low T , this result occurs only for a small t' and, as will be shown below, the opposite occurs in the presence of a realistic t' for cuprates.

The system also exhibits PS at low doping. The inset of Fig. 2 shows the PS line in a larger temperature scale. We see that PS appears with decreasing temperature, but with further cooling down it goes back to the paramagnetic phase. As a result, PS occurs only in an intermediate temperature region. This peculiar reentrant behavior was also found in Ref. 74 in the Hubbard model. The region of PS shrinks with increasing V and also by introducing $t'(< 0)$, as will be discussed in the subsection D.

The phase diagram in Fig. 2 should not be interpreted in such a way that the $dCDW$ is unstable against the dPI or BOP at low T or low δ , because we perform a stability analysis in the paramagnetic phase. Rather, Fig. 2 indicates a hierarchy for different charge instabilities, i.e., the outer the critical line is, the stronger the tendency toward the corresponding instability is.

It requires highly accurate numerics to determine precisely a modulation vector \mathbf{q} of each order along its outer critical line because of a rather flat structure of the susceptibility in momentum space, especially for the dPI . Therefore considering our achieved numerical accuracy we present in Fig. 3 modulation vectors of each instability, for which the absolute value of the corresponding eigenvalue of $D_{ab}^{-1}(\mathbf{q}, 0)$ becomes less than $10^{-4}t$ on its outer critical line. The width of such a \mathbf{q} region, at a fixed temperature, implies how sharp

the susceptibility is in momentum space. Since modulation vectors of each instability are computed along its outer critical line, each critical temperature shown in Fig. 3 corresponds to a certain critical doping rate, which can be read off from Fig. 2. Although Fig. 3 is presented only along the axis $(\pi, 0)$ - (π, π) -($0, 0$)- $(\pi, 0)$, we scanned the whole \mathbf{q} region of the Brillouin zone and checked numerically that instabilities indeed occur along that axis.

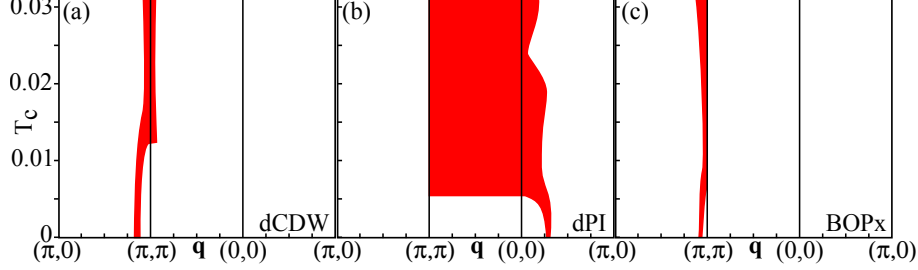


FIG. 3: (Color online) Modulation vectors for d CDW (left panel), d PI (middle panel), and BOP_x (right panel) along the corresponding outer critical line in Fig. 2. For each critical temperature, the critical doping rate can be read off from Fig. 2. Because of symmetry, the results along the direction of $(0, \pi)$ - (π, π) are the same as those along the $(\pi, 0)$ - (π, π) direction for the d CDW and d PI.

In Fig. 3 (a) we show the result for the d CDW along its outer critical line in Fig. 2. At high critical temperature (i.e., low critical doping rate) the instability occurs at $\mathbf{q} = (\pi, \pi)$, and with lowering temperature the modulation vector shifts from (π, π) and becomes incommensurate. In Fig. 3 (c) we plot the corresponding modulation vector of the BOP_x . At low T , the modulation vector \mathbf{q} slightly shifts from (π, π) and the BOP_x becomes incommensurate, as in the case of the d CDW. At high T , \mathbf{q} is located at (π, π) , but in contrast to the case of the d CDW, the \mathbf{q} region is not extended on the side of the direction of (π, π) -($0, 0$). This is because the eigenvector of the BOP_x does not exist there, instead, the eigenvector of the full susceptibility [Eq. (16)] changes to that corresponding to the d PI. A modulation vector of the BOP_{xy} appears only along the axis (π, π) -($0, 0$). Its T_c dependence is very similar to that of BOP_x , but the labels $(\pi, 0)$ and $(0, 0)$ in Fig. 3 (c) should be replaced by $(0, 0)$ and $(\pi, 0)$, respectively.

The corresponding result for the d PI is shown in Fig. 3 (b), which looks very different from those for the d CDW and BOP. In fact, for $t' = 0$, the static electronic polarizability of

the d PI has a special feature, which was already noted in Ref. 23 in a different context. To see this we rewrite Eq. (24) in a different form,

$$\Pi_{d\text{PI}}(\mathbf{q}, 0) = -\frac{1}{N_s} \sum_{\mathbf{k}} n_F(\epsilon_{\mathbf{k}}) \left[\frac{\gamma_{d\text{PI}}^2(\mathbf{q}, \mathbf{k})}{\epsilon_{\mathbf{k}} - \epsilon_{\mathbf{k}+\mathbf{q}}} + \frac{\gamma_{d\text{PI}}^2(-\mathbf{q}, \mathbf{k})}{\epsilon_{\mathbf{k}} - \epsilon_{\mathbf{k}-\mathbf{q}}} \right]. \quad (32)$$

When \mathbf{q} lies along the diagonal direction $\mathbf{q} \parallel (q, q)$, we find after some algebra

$$\Pi_{d\text{PI}}(\mathbf{q}, 0) = \frac{8\Delta^2}{(t\delta + 2\Delta)N_s} \sum_{\mathbf{k}} n_F(\epsilon_{\mathbf{k}}) \cos \frac{k_x + k_y}{2} \tan \frac{k_x - k_y}{2} \sin \frac{k_x - k_y}{2}, \quad (33)$$

that is, the static d PI susceptibility [Eq. (23)] does not depend on \mathbf{q} for any momentum along the diagonal direction. This result holds for any carrier density and any temperature. Therefore, if the d PI takes place for a vector \mathbf{q} in the diagonal direction, the susceptibility diverges simultaneously at all \mathbf{q} along the diagonal direction. The full susceptibility [Eq. (16)] actually shows that feature in Fig. 3 (b). Furthermore, this flat feature of the susceptibility extends more away from the diagonal direction. The \mathbf{q} region along $(0,0)$ - $(\pi,0)$ shrinks at $T_c \approx 0.024$ in Fig. 3 (b), which results from the proximity to PS, as will be discussed in the subsection C. While the susceptibility is always flat along the diagonal direction of \mathbf{q} , the susceptibility shows a peak at a modulation vector along $(0,0)$ - $(\pi,0)$ at low T . The \mathbf{q} region has a sharp boundary at (π, π) in Fig. 3 (b) and the d PI does not have any possible modulation vector along the $(\pi,0)$ - (π, π) direction. This is because the eigenvector corresponding to the d PI is not realized along $(\pi,0)$ - (π, π) , instead, the BOP_x eigenvector appears there. This property may be understood also in terms of the effective susceptibilities. Equation (29) indicates that if $\chi_{d\text{PI}}^{-1}(\mathbf{q}', 0)$ becomes zero, either $\chi_{\text{BOP}_x}^{-1}(\mathbf{q}', 0)$ or $\chi_{\text{BOP}_y}^{-1}(\mathbf{q}', 0)$ should be already negative, since in general χ_{BOP_x} is not equal to χ_{BOP_y} for a momentum along $(\pi,0)$ - (π, π) , except for $\mathbf{q}' = (\pi, \pi)$ where both $\chi_{\text{BOP}_x}^{-1}(\mathbf{q}', 0)$ and $\chi_{\text{BOP}_y}^{-1}(\mathbf{q}', 0)$ can become zero simultaneously. Therefore a possible instability of the d PI along $(\pi,0)$ - (π, π) is replaced by the BOP_x .

The \mathbf{q} -independence of $\Pi_{d\text{PI}}$ along the diagonal direction leads to another special feature. As we mentioned at the end of Sec. II, the onset temperature of the BOP with $\mathbf{q} = (\pi, \pi)$ is the same as that of the d PI with $\mathbf{q} = (\pi, \pi)$ [Eqs. (30) and (31)]. Therefore the onset temperature of the commensurate BOP becomes the same as that of the d PI with $\mathbf{q} = \mathbf{0}$, as shown in Fig. 2.

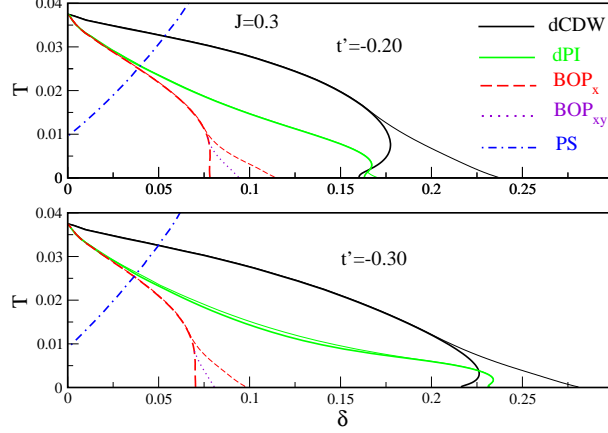


FIG. 4: (Color online) Critical temperature and doping rate for $t' = -0.20$ (upper panel) and $t' = -0.30$ (lower panel). The notation is the same as Fig. 2.

B. Results for finite t'

The degeneracy between the dPI and BOP seen in Fig. 2 is lifted by introducing t' . The upper and lower panels in Fig. 4 show the results for $t' = -0.20$ and -0.30 , respectively. While the BOP instability is always restricted to a lower doping region, the dPI becomes favorable in a wider doping region. Near half-filling the dPI and BOP are still almost degenerate because, as seen from Eq. (12), the hopping integral t' is renormalized to be $t'r_0 \propto t'\delta$ and becomes irrelevant close to half-filling. The BOP_x and BOP_{xy} are always degenerate as far as they exhibit a commensurate instability. Their degeneracy is lifted when their modulation vector becomes incommensurate at low temperature.

As shown in Fig. 4, the doping region of the commensurate $dCDW$ instability is extended by the presence of t' and an incommensurate $dCDW$ becomes dominant at high δ and low critical temperature. On the other hand, PS is suppressed by introducing t' . The critical line for PS bends back to zero doping for high T (not shown) in a way similar to the case for $t' = 0$ (inset of Fig. 2).

The modulation vector of each instability is shown in the upper and middle row in Fig. 5 for $t' = -0.20$ and -0.30 , respectively, along the corresponding outer critical line in Fig. 4. Both $dCDW$ [Figs. 5 (a) and (d)] and BOP_x [Figs. 5 (c) and (f)] show an instability at $\mathbf{q} = (\pi, \pi)$ for high critical temperature, and becomes incommensurate for low critical temperature. These features are the same as those seen in Figs. 3 (a) and (c). Results of BOP_{xy} are essentially the same as those of BOP_x , but the labels $(\pi, 0)$ and $(0, 0)$ should be

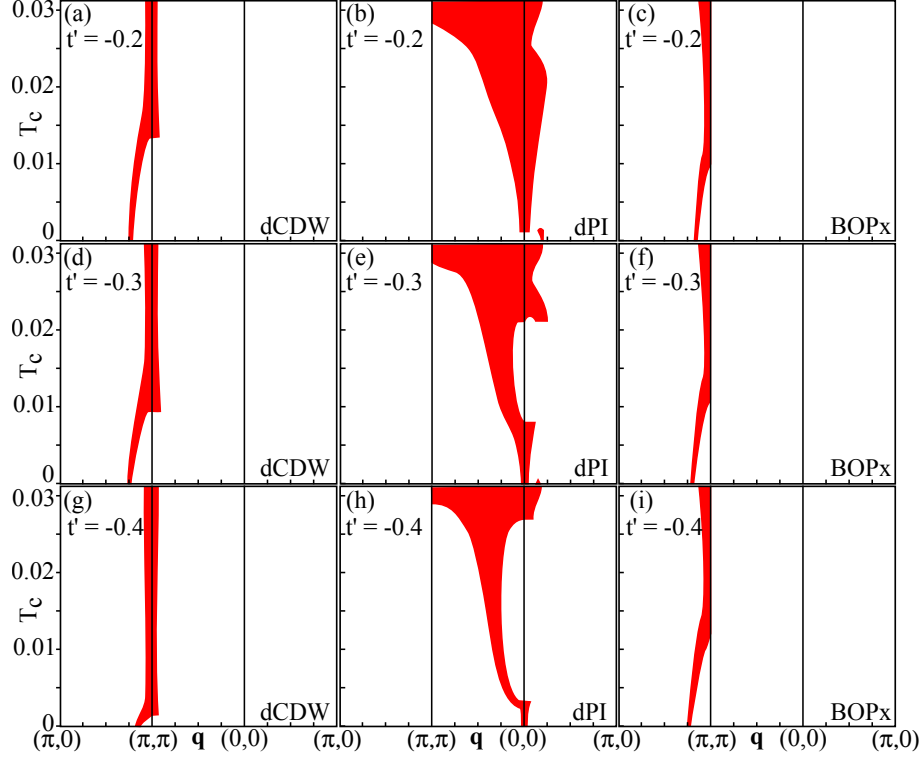


FIG. 5: (Color online) Modulation vectors for $d\text{CDW}$ (left panels), $d\text{PI}$ (middle panels), and BOP_x (right panels) for $t' = -0.20$ (upper row), $t' = -0.30$ (middle row), and $t' = -0.40$ (lower row) along the outer critical line of the corresponding order for each t' in Fig. 4 and Fig. 6 (middle).

interchanged in Figs. 5 (c) and (f).

Figs. 5 (b) and (e) show results for the $d\text{PI}$. They are very different from Fig. 3 (b), except for a region of high critical temperature near $T_c \approx 0.03$, namely the doping region $0 < \delta_c \lesssim 0.02$, where the effect of t' becomes irrelevant. For $t' = -0.20$ [Fig. 5 (b)], as the critical temperature decreases, the \mathbf{q} region shrinks around $\mathbf{q} = (0,0)$ and the $d\text{PI}$ tends to become commensurate. Close to zero temperature, however, a tendency toward an incommensurate $d\text{PI}$ appears in the $(0,0)$ - $(\pi,0)$ direction. This incommensurate feature is also seen more clearly for $t' = 0$ at low T [Fig. 3 (b)], and disappears quickly with increasing t' . It becomes nearly invisible for $t' = -0.30$ in our temperature scale. For $t' = -0.30$, the \mathbf{q} region shrinks first around $\mathbf{q} = (0,0)$ with decreasing the critical temperature. In the intermediate temperature range, $0.021 \gtrsim T_c \gtrsim 0.008$, the modulation vector becomes slightly incommensurate along the diagonal. This deviation from the commensurate vector is also barely visible in the bottom panel of Fig. 4, where the incommensurate $d\text{PI}$ line separates

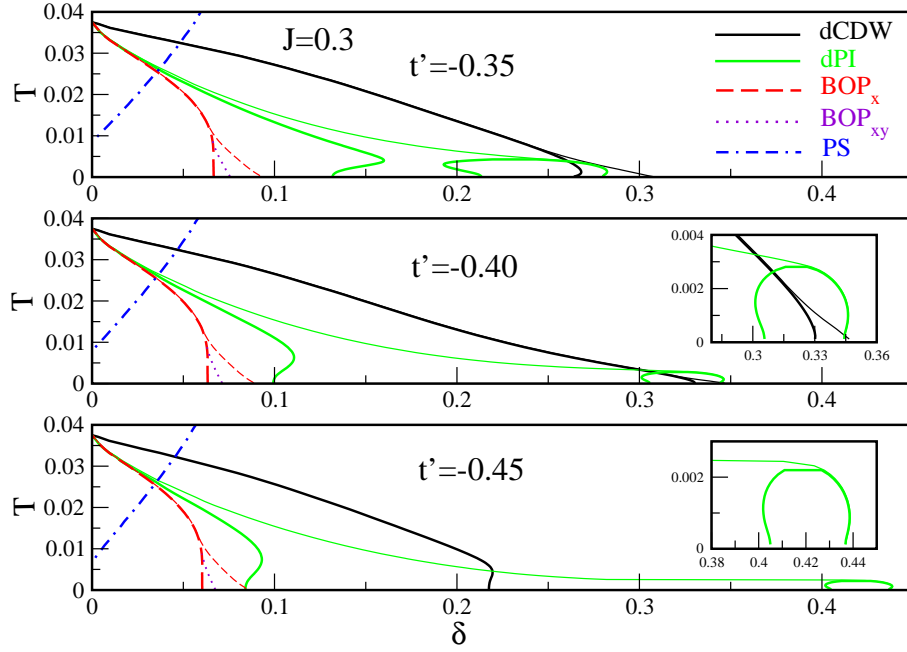


FIG. 6: (Color online) The same plot as Fig. 4, but for different choices of t' : $t' = -0.35$ (top panel), $t' = -0.40$ (middle panel), and $t' = -0.45$ (bottom panel). In the latter two cases the phase diagram in a high doping region is magnified in the inset.

very slightly from the commensurate dPI in the corresponding temperature region. For $T_c \lesssim 0.008$, the dPI becomes fully commensurate.

The phase diagram close to half-filling does not depend essentially on a choice of t' . In fact, the critical lines for the BOP and PS do not change much even for a further larger t' . However, we find that tendencies toward $dCDW$ and dPI have strong t' dependence. In Fig. 6 we present the phase diagram for $t' = -0.35$, -0.40 , and -0.45 . First we focus on the $dCDW$ for $t' = -0.35$ and -0.40 . The instability extends to a higher doping region with increasing t' and the commensurate $dCDW$ tends to become more favorable even at low T . The doping region of the $dCDW$, however, starts to decrease quickly for $|t'| > 0.41$, as can be seen in the result for $t' = -0.45$.

In contrast to the $dCDW$, the outer critical line for the dPI extends to higher doping with increasing t' . For $t' = -0.35$, an incommensurate dPI becomes dominant in a wide doping region ($0.05 \lesssim \delta \lesssim 0.25$). While the commensurate dPI is realized for $\delta \lesssim 0.16$ and $\delta \gtrsim 0.19$, it does not occur between these two doping regions. This feature is more evident for $t' = -0.40$ [Fig. 6 (middle panel)]. In a wide doping region ($0.10 \lesssim \delta \lesssim 0.30$) the

commensurate d PI does not occur and only an incommensurate d PI is possible. However in a high doping region ($0.30 \lesssim \delta \lesssim 0.35$), the commensurate d PI shows up again; see the inset in Fig. 6 (middle panel). These peculiar features of the d PI are due to the presence of the van Hove singularity around $\delta = 0.33$, where the d -wave weighted density of states,⁷⁵ which is defined by $\lim_{\mathbf{q} \rightarrow \mathbf{0}} \Pi_{d\text{PI}}(\mathbf{q}, 0)$ in Eq. (24), is enhanced, favoring the instability at $\mathbf{q} = (0, 0)$. In an intermediate doping region, the d -wave density of states is suppressed and the d PI with a finite \mathbf{q} becomes more favorable. Closer to half-filling, however, the d -wave density of states is again enhanced because of narrowing the band width upon approaching half-filling, leading to a recovery of the commensurate d PI for $\delta \lesssim 0.10$. For $t' = -0.45$ these features are more emphasized. Figure 6 (bottom panel) shows that the commensurate d PI occurs both, close to half-filling and around van Hove filling ($\delta = 0.42$), and these two regions are connected by the critical line of an incommensurate d PI. The commensurate d PI close to half-filling and in a high doping region was also found in the slave-boson mean-field theory.³⁴

In Fig. 5 we compare the modulation vector of each instability for $t' = -0.20, -0.30$, and -0.40 . With increasing t' , the d CDW tends to be more commensurate even at low critical temperature. For the d PI, on the other hand, a large t' tends to favor an incommensurate modulation along the diagonal direction of the Brillouin zone in an intermediate range of a critical temperature, and the commensurate d PI can be realized only at high and low critical temperature, corresponding to a doping region close to half-filling and around van Hove filling, respectively. The modulation vectors of the BOP_x (and also BOP_{xy}) do not depend much on a choice of t' .

C. Mutual interaction among different modes

Because of the renormalization of the bosonic propagators due to the coupling to electronic bubbles [Eq. (16)], one would expect in general some coupling among different modes. This effect actually appears for modulation vectors of the d PI. There is a dip on the side of the region of $(0, 0)$ - $(\pi, 0)$ at $T_c \approx 0.024$ in Fig. 3 (b), and $T_c \approx 0.025$ and 0.026 in Figs. 5 (b) and (e), respectively. This dip occurs near the temperature where the critical lines of the d PI and PS cross each other (see Figs. 2 and 4). Moreover, we checked that the dip in question does not appear in results obtained from the effective susceptibility of the d PI [Eq. (23)].

Therefore a tendency toward PS plays a role in the suppression of the incommensurate feature of the d PI along $(0,0)$ - $(\pi,0)$.

Except for the above feature, we checked that our results (Figs. 2-6) are nearly the same as those determined by the effective susceptibilities [Eqs. (20), (21), (23), and (25)]. In this sense, the coupling among different bosonic fluctuations is rather weak at least in leading order.

D. Effect of the V -term and stability of phase separation

We checked that the results for d CDW, d PI, and BOP are almost intact for different choices of V (≥ 0) and that an additional instability such as the usual checkerboard charge density wave does not occur at least for $V \leq 1$ for any doping rate.^{25,76} Furthermore, the reentrant critical line of PS (inset of Fig. 2) is a robust feature. However, it is a subtle issue whether PS actually occurs at $T = 0$. The result depends on choices of V , t' , and J . For $t' = 0$ and $J = 0.3$, we found that PS at $T = 0$ occurs for $\delta \lesssim 0.08$ (0.025) at $V = 0$ (0.1) and vanishes already for $V \gtrsim 0.2$. When t' is introduced, PS is strongly suppressed even at $V = 0$, for example, it occurs at $T = 0$ only for $\delta \lesssim 0.01$ for $t' = -0.35$. A smaller J also suppresses PS, and for the special case of $J = 0$ no PS is observed at $T = 0$ for any V (≥ 0) and t' (≤ 0).

IV. CONCLUSION

Applying a large- N expansion formulated in the path integral representation of the t - J model, we have analyzed all possible charge instabilities of the paramagnetic phase, and have elucidated the phase diagram in the doping and temperature plane for a sequence of t' . We have found that d CDW, d PI, BOP, and PS are the most important charge instabilities. The first two instabilities appear in a wide doping region. The d CDW usually becomes the leading instability and the d PI occurs as a next leading one with a strong tendency to become incommensurate. In the presence of a large t' , however, we have found that the d PI becomes the leading instability in a high doping region. Considering the high complexity of the t - J model, it is beyond the scope of the present study to address which charge instability would become ultimately the leading one. Rather, the present stability analysis on charge

instabilities of the paramagnetic state was motivated by active studies on the PG in cuprates in terms of various charge fluctuations, and we have provided a microscopic basis of possible charge fluctuations in doped Mott insulators. We first compare our results with literature and then discuss implications for cuprate superconductors.

Taking into account a number of papers about charge stripes in cuprates,^{16,17} it may be surprising that we do not detect stripe tendencies in our formalism, which exclusively favors charge instabilities. If the t - J model would exhibit a tendency to charge stripes order, it might be a consequence of a coupling with incommensurate magnetic modes, which could appear in the next-to-leading order [$O(1/N)$] in the present scheme. A charge-stripe solution was actually obtained in the t - J model with $t' = 0$ in the DMRG study,^{47,48,77} which however contradicts other studies.^{56,78} In the presence of t' , on the other hand, most of numerical studies in the t - J model reported that the charge stripe solution becomes unstable.^{49,50} Our results, therefore, agree to major literature.

Interestingly, the BOP _{$x(y)$} shares the same feature as stripe order from a symmetry point of view. When \mathbf{q} shifts away from (π, π) , \mathbf{q} is located only along the $q_{y(x)}$ direction and thus the BOP _{$x(y)$} breaks both orientational and translational symmetry of the lattice. In fact such an incommensurate BOP _{$x(y)$} instability is found to occur up to $\delta \sim 0.10$; see Figs. 2, 4, and 6. While the BOP has not been discussed much so far, the BOP was also obtained in other studies in the t - J model.²³⁻²⁵

As discussed in Sec. III.D, PS at $T = 0$ strongly depends on a choice of V , t' , and J . However it is a robust feature that PS occurs in an intermediate temperature region. This property for a finite T has not been discussed so far except for Ref. 74 in the Hubbard model, probably because various numerical simulations are usually coded only at zero temperature. Interestingly, the reentrant critical line of PS (see the inset of Fig. 2) was interpreted as a source to generate a strong forward scattering channel of the electron-phonon vertex which emerges only at finite T .⁷⁴

While the commensurate d PI ($\mathbf{q} = \mathbf{0}$) was already found in the t - J ³⁴ and Hubbard³⁷ models, an incommensurate d PI ($\mathbf{q} \neq \mathbf{0}$) started to be discussed quite recently.⁷⁰⁻⁷³ We have obtained that the static d -wave electronic polarizability [Eq. (33)] does not depend on \mathbf{q} for any momentum along the Brillouin zone diagonal, which holds for any temperature and any electron density as long as t' is zero. In our model, this feature remains even for a finite t' near half-filling since t' is effectively reduced by a factor of δ . Our result shown in the

inset of Fig. 6 (bottom panel) may be best compared with existing results, since they were obtained in a weak coupling analysis.^{70–73} At hole density below van Hove filling ($\delta \lesssim 0.42$), the leading instability is an incommensurate d PI and its modulation vector is located along the $(0,0)$ - (π,π) direction, which agrees with literature.^{70–73} At hole density above van Hove filling we have obtained the d PI with $\mathbf{q} = \mathbf{0}$, while Ref. 72 showed that the static electronic polarizability of the d PI has a peak along the $(0,0)$ - $(\pi,0)$ direction at least at $T = 0$. In our case, an incommensurate peak along the $(0,0)$ - $(\pi,0)$ direction indeed develops as seen in Figs. 3 (b), 5 (b) for a small t' , but it develops below extremely low temperature for a large t' . This effect is not visible in Fig. 6 (bottom).

In the $1/N$ expansion, the d CDW is the leading instability in most of cases, in agreement with previous studies.^{23–25} We have found that close to the d CDW, the d PI also exists in a wide doping region. Therefore fluctuations associated with both d CDW and d PI are expected to be important for temperatures above the onset of the d CDW. The mutual interaction between d CDW and d PI seems rather weak at least in leading order because both, the full calculation [Eq. (16)] and effective susceptibilities [Eqs. (20), (21), (23), and (25)], give nearly the same results. Given that the presence of t' is usually assumed for cuprates and our critical lines of d CDW and d PI have the same doping dependence of the PG temperature, furthermore with a comparable temperature if $t \approx 500$ meV, it is interesting to study each fluctuation effect on the electronic property. In fact, existing work already showed interesting results, but with some open questions. The phenomenological study assuming the d CDW showed that essential features of the PG are well captured.¹⁰ However fluctuation effects were not considered in Ref. 10. In a perturbative calculation of the electron self-energy due to a coupling to d CDW fluctuations in the t - J model, a pseudogap is obtained in the electronic spectral function, which shares many important features with experimental data.^{29–31} Moreover the same analysis was also applied to the explanation of anisotropic scattering rate of quasi-particles⁷⁹ observed in angle-dependent magnetoresistance experiments.⁸⁰ However, no calculation was performed beyond the perturbative analysis. On the other hand, in a perturbative calculation for d PI fluctuations centered around $\mathbf{q} = (0,0)$, a splitting of the spectral function near the Fermi energy was obtained, reminiscent of a pseudogap.⁸¹ Going beyond the perturbation theory and summing up all diagrams in the Gaussian fluctuation regime, however, instead of a splitting, the spectral function exhibits a broad single peak centered at the Fermi energy with a strong \mathbf{k} dependence of d -wave symmetry.⁸¹ The spec-

trum in the Ginzburg region⁸² is an open question. Furthermore, the role of incommensurate d PI fluctuations on a pseudogap phenomenon remains elusive.

The d PI couples directly with xy anisotropy such as due to a lattice structure and an external strain. While the d PI changes to a crossover phenomenon in such a case, the anisotropy can be strongly enhanced by the underlying d PI fluctuations as already discussed.^{34,40} The same idea is also discussed for iron-pnictide superconductors near the structural phase transition from the tetragonal to orthorhombic phase.⁸³ Given that lattice anisotropy frequently exists in cuprates, the relevance of the d PI channel in the t - J model suggests important implications for understanding cuprate superconductors, not only for Y-based^{11,41–45} but also for La-based^{34,84–86} compounds.

For a large t' , the commensurate d PI appears in a heavily overdoped region around van Hove filling ($\delta \approx 0.3 - 0.45$ in Fig. 6). While our critical line exhibits reentrant behavior at low T , the canonical model for the d PI^{75,87} suggests that the reentrant behavior is preempted by a first order transition as a function of the chemical potential, or equivalently a phase separation as a function of doping, as far as the d PI occurs at $\mathbf{q} = \mathbf{0}$. It is known that $\text{Sr}_3\text{Ru}_2\text{O}_7$ exhibits the d PI in a magnetic field.^{88–90} In addition, a highly overdoped region in cuprates, where no superconducting and antiferromagnetic instabilities are expected, may also provide an opportunity to explore the d PI.

Acknowledgments

The authors thank C. Gazza, T. Holder, C. Husemann, W. Metzner, S. Sorella, and R. Zeyher for valuable discussions. M. B. thanks Consejo Nacional de Investigaciones Científicas y Técnicas (CONICET) for financial support. A. G. thanks the National Institute for Materials Science (NIMS), where this work was initiated, and the Max-Planck-Institute for hospitality. H. Y. was supported by a Grant-in-Aid for Scientific Research from Monokasho and the Alexander von Humboldt Foundation.

¹ T. Timusk and B. Statt, Rep. Prog. Phys. **62**, 61 (1999).

² M. R. Norman, D. Pines and C. Kallin, Adv. Phys. **54**, 715 (2005).

³ A. Damascelli, Z. Hussain, and Z. X. Shen, Rev. Mod. Phys. **75**, 473 (2003).

- ⁴ M. R. Norman, H. Ding, M. Randeris, J. C. Campuzano, T. Yokoya, T. Takeuchi, T. Takahashi, T. Mochiku, K. Kadowaki, P. Guptasarma, and D. G. Hinks, *Nature (London)* **392**, 157 (1998).
- ⁵ V. J. Emery and S. A. Kivelson, *Nature* **374**, 434 (1995).
- ⁶ M. R. Norman, A. Kanigel, M. Randeria, U. Chatterjee, and J. C. Campuzano, *Phys. Rev. B* **76**, 174501 (2007).
- ⁷ I. M. Vishik, W. S. Lee, R.-H. He, M. Hashimoto, Z. Hussain, T. P. Devereaux, and Z.-X. Shen, *New J. Phys.* **12**, 105008 (2010).
- ⁸ T. Kondo, Y. Hamaya, A. D. Palczewski, T. Takeuchi, J. S. Wen, Z. J. Xu, G. Gu, J. Schmalian, and A. Kaminski, *Nat. Phys.* **7**, 21 (2011).
- ⁹ T. Yoshida, M. Hashimoto, I. M. Vishik, Z.-X. Shen, and A. Fujimori, *J. Phys. Soc. Jpn.* **81**, 011006 (2012).
- ¹⁰ S. Chakravarty, R. B. Laughlin, D. K. Morr, and C. Nayak, *Phys. Rev. B* **63**, 094503 (2001).
- ¹¹ H. Yamase, *Phys. Rev. B* **79**, 052501 (2009).
- ¹² C. Castellani, C. Di Castro, and M. Grilli, *Phys. Rev. Lett.* **75**, 4650 (1995).
- ¹³ F. Becca, M. Tarquini, M. Grilli, and C. Di Castro, *Phys. Rev. B* **54**, 12443 (1996).
- ¹⁴ M. Hashimoto, R.-H. He, K. Tanaka, J. -P. Testaud, W. Meevasana, R. G. Moore, D. Lu, H. Yao, Y. Yoshida, H. Eisaki, T. P. Devereaux, Z. Hussain, and Z.-X. Shen, *Nat. Phys.* **6**, 414 (2010).
- ¹⁵ R.-H. He, M. Hashimoto, K. Karapetyan, J. D. Koralek, J. P. Hinton, J. P. Testaud, V. Nathan, Y. Yoshida, H. Yao, K. Tanaka *et al.*, *Science* **311**, 1579 (2011).
- ¹⁶ S. A. Kivelson, I. P. Bindloss, E. Fradkin, V. Oganessian, J. M. Tranquada, A. Kapitulnik, and C. Howald, *Rev. Mod. Phys.* **75**, 1201 (2003).
- ¹⁷ M. Vojta, *Adv. Phys.* **58**, 699 (2009).
- ¹⁸ V. J. Emery and S. A. Kivelson, *Physica C* **209**, 597 (1993).
- ¹⁹ K.-Y. Yang, T. M. Rice and F.-C. Zhang, *Phys. Rev. B* **73**, 174501 (2006).
- ²⁰ C. M. Varma, *Phys. Rev. Lett.* **83**, 3538 (1999); *Phys. Rev. B*, **73**, 155113 (2006).
- ²¹ I. Affleck and J. B. Marston, *Phys. Rev. B* **37**, 3774 (1988).
- ²² I. Affleck and J. B. Marston, *Phys. Rev. B* **39**, 11538 (1989).
- ²³ D. Morse and T. Lubensky, *Phys. Rev. B* **43**, 10436 (1991).
- ²⁴ E. Cappelluti and R. Zeyher, *Phys. Rev. B* **59**, 6475 (1999).
- ²⁵ A. Foussats and A. Greco, *Phys. Rev. B* **70**, 205123 (2004).

- ²⁶ P. W. Leung, Phys. Rev. B **62**, R6112 (2000).
- ²⁷ A. Macridin, M. Jarrell, and Th. Maier, Phys. Rev. B **70**, 113105 (2004).
- ²⁸ X. Lu, L. Chioncel, and E. Arrigoni, Phys. Rev. B **85**, 125117 (2012).
- ²⁹ A. Greco, Phys. Rev. Lett. **103**, 217001 (2009).
- ³⁰ M. Bejas, G. Buzon, A. Greco, and A. Foussats, Phys. Rev. B **83**, 014514 (2011).
- ³¹ A. Greco and M. Bejas, Phys. Rev. B **83**, 212503 (2011).
- ³² I. J. Pomeranchuk, Sov. Phys. JETP **8**, 361 (1959).
- ³³ S. A. Kivelson, E. Fradkin, and V. J. Emery, Nature (London) **393**, 550 (1998).
- ³⁴ H. Yamase and H. Kohno, J. Phys. Soc. Jpn. **69**, 332 (2000); **69**, 2151 (2000).
- ³⁵ A. Miyanaga and H. Yamase, Phys. Rev. B **73**, 174513 (2006).
- ³⁶ B. Edegger, V. N. Muthukumar, and C. Gros, Phys. Rev. B **74**, 165109 (2006).
- ³⁷ C. J. Halboth and W. Metzner, Phys. Rev. Lett. **85**, 5162 (2000).
- ³⁸ I. Grote, E. Körding, and F. Wegner, J. Low Temp. Phys. **126**, 1385 (2002); V. Hankevych, I. Grote, and F. Wegner, Phys. Rev. B **66**, 094516 (2002).
- ³⁹ J. Buenemann, T. Schickling, and F. Gebhard, Europhys. Lett. **98**, 27006 (2012).
- ⁴⁰ S. Okamoto, D. Sénéchal, M. Civelli, and A.-M. Tremblay, Phys. Rev. B **82**, 180511 (2010).
- ⁴¹ V. Hinkov, P. Bourges, S. Pailhès, Y. Sidis, A. Ivanov, C. D. Frost, T. G. Perring, C. T. Lin, D. P. Chen, and B. Keimer, Nat. Phys. **3**, 780 (2007).
- ⁴² V. Hinkov, D. Haug, B. Fauqué, P. Bourges, Y. Sidis, A. Ivanov, C. Bernhard, C. T. Lin, and B. Keimer, Science **319**, 597 (2008).
- ⁴³ R. Daou, J. Chang, D. LeBoeuf, O. Cyr-Choinière, F. Laliberté, N. Doiron-Leyraud, B. J. Ramshaw, R. Liang, D. A. Bonn, W. H. Hardy, and L. Taillefer, Nature **463**, 519 (2010).
- ⁴⁴ H. Yamase and W. Metzner, Phys. Rev. B **73**, 214517 (2006).
- ⁴⁵ A. Hackl and M. Vojta, Phys. Rev. B **80**, 220514(R) (2009).
- ⁴⁶ J. M. Tranquada, B. J. Sternlieb, J. D. Axe, Y. Nakamura, and S. Uchida, Nature (London) **375**, 561 (1995).
- ⁴⁷ S. R. White and D. J. Scalapino, Phys. Rev. Lett. **80**, 1271 (1998); **81**, 3227 (1998).
- ⁴⁸ S. R. White and D. J. Scalapino, Phys. Rev. B **61**, 6320 (2000).
- ⁴⁹ S. R. White and D. J. Scalapino, Phys. Rev. B **60**, R753 (1999).
- ⁵⁰ T. Tohyama, C. Gazza, C. T. Shih, Y. C. Chen, T. K. Lee, S. Maekawa, and E. Dagotto, Phys. Rev. B **59**, R11649 (1999).

- ⁵¹ M. Marder, N. Papanicolau, and G. C. Psaltakis, Phys. Rev. B **41**, 6920 (1990).
- ⁵² V. J. Emery, S. A. Kivelson, and H. Q. Lin, Phys. Rev. Lett. **64**, 475 (1990).
- ⁵³ C. S. Hellberg and E. Manousakis, Phys. Rev. B **61**, 11787 (2000).
- ⁵⁴ D. A. Ivanov, Phys. Rev. B **70**, 104503 (2004).
- ⁵⁵ H. Yokoyama and M. Ogata, J. Phys. Soc. Jpn. **65**, 3615 (1996).
- ⁵⁶ C. S. Hellberg and E. Manousakis, Phys. Rev. Lett. **83**, 132 (1999).
- ⁵⁷ C. T. Shih, Y. C. Chen, and T. K. Lee, Phys. Rev. B **57**, 627 (1998).
- ⁵⁸ W. O. Putikka and M. U. Luchini, Phys. Rev. B **62**, 1684 (2000).
- ⁵⁹ M. Lugas, L. Spanu, F. Becca, and S. Sorella, Phys. Rev. B **74**, 165122 (2006).
- ⁶⁰ P. W. Anderson, Science **235**, 1196 (1987).
- ⁶¹ A. Foussats, A. Greco, C. Repetto, O. P. Zandron, and O. S. Zandron, J. Phys. A **33**, 5849 (2000).
- ⁶² A. Foussats and A. Greco, Phys. Rev. B **65**, 195107 (2002).
- ⁶³ R. Zeyher and A. Greco, Eur. Phys. J. B **6**, 473 (1998).
- ⁶⁴ C. Gazza, G. Martins, J. Riera, and E. Dagotto, Phys. Rev. B **59**, R709 (1999).
- ⁶⁵ J. Hubbard, Proc. R. Soc. London A **276**, 238 (1963).
- ⁶⁶ Since f is proportional to X^{0p} , f and f^\dagger do not fulfill the fermionic commutation rules. But after the expansion with respect to δR in the Lagrangian, f behaves as a fermion and its non-interacting propagator is given by a usual one, Eq. (11). The price paid is the generation of various interaction terms between f and the bosonic field δX^a . For details see Refs. 25 and 62.
- ⁶⁷ P. A. Lee, N. Nagaosa, and X.-G. Wen, Rev. Mod. Phys. **78**, 17 (2006).
- ⁶⁸ J. Merino, A. Greco, R. H. McKenzie, and M. Calandra, Phys. Rev. B **68**, 245121 (2003).
- ⁶⁹ M. Bejas, A. Greco, and A. Foussats, Phys. Rev. B **73**, 245104 (2006).
- ⁷⁰ M. A. Metlitski and S. Sachdev, Phys. Rev. B **82**, 075127 (2010).
- ⁷¹ M. A. Metlitski and S. Sachdev, New J. Phys. **12**, 105007 (2010).
- ⁷² T. Holder and W. Metzner, Phys. Rev. B **85**, 165130 (2012).
- ⁷³ C. Husemann and W. Metzner, arXiv: 1203.2887.
- ⁷⁴ E. Koch and R. Zeyher, Phys. Rev. B **70**, 094510 (2004).
- ⁷⁵ H. Yamase, V. Oganesyan, and W. Metzner, Phys. Rev. B **72**, 035114 (2005).
- ⁷⁶ The value of V_c presented in Fig. 7 in Ref. 25 should be read as that of $V_c/2$.
- ⁷⁷ P. Corboz, S. R. White, G. Vidal, and M. Troyer, Phys. Rev. B **84**, 041108(R) (2011).

- ⁷⁸ W. Hu, F. Becca, and S. Sorella, Phys. Rev. B **85**, 081110 (2012).
- ⁷⁹ G. Buzon and A. Greco, Phys. Rev. B **82**, 054526 (2010).
- ⁸⁰ M. Abdel-Jawad, M. Kennett, L. Balicas, A. Carrington, A. Mackenzie, R. McKenzie, and N. Hussey, Nat. Phys. **2**, 821 (2006).
- ⁸¹ H. Yamase and W. Metzner, Phys. Rev. Lett. **108**, 186405 (2012).
- ⁸² V. L. Ginzburg, Sov. Phys. Sol. State **2**, 1824 (1960).
- ⁸³ I. R. Fisher, L. Degiorgi, and Z. X. Shen, Rep. Prog. Phys. **74**, 124506 (2011).
- ⁸⁴ H. Yamase and H. Kohno, J. Phys. Soc. Jpn. **70**, 2733 (2001).
- ⁸⁵ H. Yamase, J. Phys. Soc. Jpn. **71**, 1154 (2002).
- ⁸⁶ H. Yamase, Phys. Rev. B **75**, 014514 (2007).
- ⁸⁷ I. Khavkine, C.-H. Chung, V. Oganessian, and H.-Y. Kee, Phys. Rev. B **70**, 155110 (2004).
- ⁸⁸ S. A. Grigera, P. Gegenwart, R. A. Borzi, F. Weickert, A. J. Schofield, R. S. Perry, T. Tayama, T. Sakakibara, Y. Maeno, A. G. Green, and A. P. Mackenzie, Science **306**, 1154 (2004).
- ⁸⁹ R. A. Borzi, S. A. Grigera, J. Farrell, R. S. Perry, S. J. S. Lister, S. L. Lee, D. A. Tennant, Y. Maeno, and A. P. Mackenzie, Science **315**, 214 (2007).
- ⁹⁰ A. W. Rost, R. S. Perry, J.-F. Mercure, A. P. Mackenzie, and S. A. Grigera, Science **325**, 1360 (2009).